Cross-correlation measurement techniques for cavity-based axion and weakly interacting slim particle searches

Stephen R. Parker,[1,*] Ben T. McAllister,[1] Eugene N. Ivanov,[2] and Michael E. Tobar[1]

[1] *ARC Centre of Excellence for Engineered Quantum Systems, School of Physics, The University of Western Australia, Crawley 6009, Australia*

[2] *School of Physics, The University of Western Australia, Crawley 6009, Australia*

(Dated: December 31, 2015)

Weakly Interacting Slim Particles (WISPs), such as axions, are highly motivated dark matter candidates. The most sensitive experimental searches for these particles exploit WISP-to-photon conversion mechanisms and use resonant cavity structures to enhance the resulting power signal. For WISPs to constitute Cold Dark Matter their required masses correspond to photons in the microwave spectrum. As such, searches for these types of WISPs are primarily limited by the thermal cavity noise and the broadband first-stage amplifier noise. In this work we propose and then verify cross-correlation measurement techniques for cavity-based WISP searches. These are two channel measurement schemes where the cross-spectrum is computed, rejecting uncorrelated noise sources while still retaining correlated signals such as those generated by WISPs. One technique allows for the cavity thermal spectrum to be observed with an enhanced resolution. Another technique cross-correlates individual cavity/amplifier systems that can be spatially well-separated, thereby opening up opportunities for characterizing candidate dark matter WISP signals.

arXiv:1510.05775v2 [physics.ins-det] 29 Dec 2015

I. INTRODUCTION

Weakly Interacting Slim Particles (WISPs) are a broad class of hypothetical particles with sub-eV masses that provide elegant and compelling solutions to a host of outstanding issues in particle physics and cosmology [1]. One of the most well known WISPs, the axion, arose out of a solution to the QCD Strong CP problem [2–5] yet also makes an ideal dark matter candidate [6–9]. Other WISPs, such as the Hidden Sector Photon [10–12] (Paraphoton [13]), can also be formulated as dark matter [14, 15].

Experimental searches for these particles typically involve exploiting WISP-to-photon couplings, which provide a sensitive portal for detection with minimal model dependency. The exact mechanisms behind this coupling varies greatly between different WISPs - for example, the axion couples to two photons and axion-photon conversion can be induced by using a magnetic field to act as the second virtual photon (inverse Primakoff effect [16, 17]), while Hidden Sector Photons undergo spontaneous kinetic mixing analogous to neutrino flavour oscillations. In these processes the mass of the WISP directly translates to the frequency of the photons created. For Cold Dark Matter (CDM) WISP models the feasible mass range spans from $\sim$1 μeV to $\sim$1 meV [1, 5], which corresponds to photons within the microwave and millimetre-wave spectrums (240 MHz to 240 GHz).

Two of the most sensitive and mature techniques for WISP searches in this region are the haloscope [16, 18, 19] and Light Shining through a Wall (LSW) [20, 21] experiments. Both approaches use microwave resonant cavity structures and low noise amplifiers as their enabling technologies. Haloscopes rely on converting the local WISP dark matter flux in to photons within a cavity structure and detecting the resonantly enhanced power signal with a chain of amplifiers. LSW searches use two nominally identical cavity structures separated by an electromagnetically impenetrable barrier; one cavity is driven on resonance to generate WISPs while the second cavity functions in essence as a haloscope - although the origin of the WISPs is not galactic but rather due to WISPs from the first cavity traversing the barrier and reconverting to photons. Several microwave haloscope [22, 23] and LSW [24–28] experiments have been conducted to date, with no reports of any signals congruent with WISP detection. The majority of these searches have been conducted below 10 GHz due to a multitude of technical issues and limitations. Despite this, the higher frequency parameter space is theoretically well motivated and has even offered up some hints of possible CDM WISPs [29]. In this work we outline new readout measurement techniques for cavity-based WISP searches. It is important to emphasize that the techniques and concepts discussed are readily applicable to a broad range of WISP searches, including LSW and proposals for new types of experiments [30–37].

II. WISP CAVITY RECEIVERS

An overview of a classic WISP cavity receiver, in this case an axion haloscope, is presented in Fig. 1. A static external magnetic field is superimposed on the intrinsic (caused by thermal fluctuations) electric field of a microwave cavity such that the dot product of B_0 and E is ideally maximized. As axions traverse through the cavity and interact with the magnetic field they will convert in

* stephen.parker@uwa.edu.au

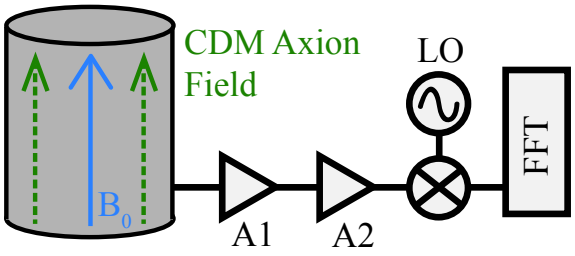

FIG. 1. Schematic of a WISP cavity receiver, in this case the prototypical axion haloscope. A1 represents the first-stage amplifier, while A2 covers all further stages of amplification. LO is the Local Oscillator used to down-convert the cavity spectrum for sampling on a Fast Fourier Transform (FFT) vector signal analyzer, or some appropriate digitizer.

to photons, resulting in a build up of power in Watts,

$$P_a = \left(\frac{g_\gamma \alpha}{\pi f_a}\right)^2 \frac{\rho_a}{m_a} V B_0^2 C \min\left(Q_L, Q_a\right), \tag{1}$$

where g_γ is a model-dependent parameter of $\mathcal{O}(1)$ [5, 38–40], α is the fine structure constant and f_a is the Peccei-Quinn symmetry-breaking energy scale [5]. The energy scale dictates the mass of the axion and the strength of its coupling to standard model particles; this is the parameter that haloscopes ultimately aim to measure or bound. The strength of the expected axion power signal also depends on the local density of axion dark matter, ρ_a. Cosmological observations provide an estimate for the local dark matter density ($0.35^{+0.08}_{-0.07}$ GeV/cm^3 [41]), however it is important to note that to date axion haloscope searches have typically only excluded CDM axions under the assumption that they constitute all of the local dark matter. It is plausible that dark matter is comprised of more than one particle species and thus the local axion dark matter density is lower than has been assumed in previous haloscope searches. This opens up the possibility of needing to repeat axion searches in already excluded regions of parameter space to check for lower density axion CDM.

The remaining factors of eq. (1) relate to the properties of the cavity used - V is the volume, Q_L is the loaded quality factor and C is a form factor [42] describing the relative overlap of the applied magnetic field and the electric field of the chosen cavity resonance, which is typically the TM_{010} mode for haloscopes (C ~0.69). The so-called axion quality factor, Q_a, describes the expected structure of a virialized CDM galactic halo axion signal, where considerations of dispersion lead to a value of $\sim 10^6$. Nonvirialized axion CDM would have a narrower linewidth (higher Q_a) [23], approaching that of a quasi-monochromatic signal.

The aim of the cavity receiver is to resolve any signal generated by WISPs (such as axions, eq. (1)) over the intrinsic noise of the measurement system with some level of confidence. The two dominating noise contributions arise from the thermal noise of the cavity and the white technical noise of the first stage amplifier (A1), which we model as a noise source attached to a noiseless gain stage. Here we assume that the cavity and amplifier are critically coupled and separated by a circulator in thermal equilibrium. We can express the Power Spectral Density (PSD, in units Watts/Hz) of cavity thermal fluctuations at the input of the amplifier as

$$\mathrm{S_P^{cav}} = k_B \mathrm{T}_0, \tag{2}$$

where T_0 is the physical temperature of the cavity. If the cavity is connected directly to the amplifier, without the use of a circulator, then eq. (2) becomes shaped by a Lorentzian profile dictated by the transmission coefficient of the cavity. Similarly the PSD of broadband amplifier technical noise at its input is given by

$$\mathrm{S_P^{amp}} = k_B \mathrm{T_{eff}}, \tag{3}$$

where $\mathrm{T_{eff}}$ is the effective noise temperature of the first stage amplifier. This is assuming that the first stage amplifier and data acquisition system are operating at a frequency outside of the flicker noise regime for the amplifier. The gain of the first stage amplifier suppresses the noise contributions of the later stage amplifiers to negligible levels [19]. To illustrate the concepts that follow we treat the WISP signal as monochromatic, such that the PSD is given by

$$\mathrm{S_P^{sig}} = \tau_{\mathrm{meas}} \mathrm{P_{sig}}, \tag{4}$$

where τ_{meas} is the measurement or observation time. The Signal-to-Noise Ratio (SNR) for a WISP cavity receiver is then simply the ratio of spectral densities, eqs. (2)-(4):

$$\mathrm{SNR} = \frac{\mathrm{S_P^{sig}}}{\mathrm{S_P^{cav}} + \mathrm{S_P^{amp}}}. \tag{5}$$

From this initial SNR one can then average over m spectrums, thereby reducing the standard deviation (or measurement error) by $\sqrt{m}$.

III. CROSS-CORRELATION

Cross-correlation measurements [43–45] have been used for many years in the characterization of low noise devices such as microwave amplifiers and oscillators. The technique involves computing the cross-correlation function of two signals; any fluctuations that are not correlated between the signals are rejected, what remains is any process that is present in both signals and correlated. Applied correctly this provides a powerful tool to reduce or eliminate the noise contributions of measurement systems. Cross-correlation measurements are practically limited by the level of isolation between the two measurement channels, typically it is possible to achieve rejection of the uncorrelated noise on the order of 20 - 30 dB.

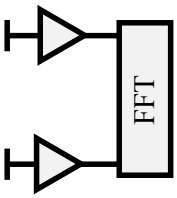

FIG. 2. Schematic of the measurement scheme used to demonstrate principles of cross-correlation. Both amplifiers were SR560 low-noise pre-amplifier models from Stanford Research Systems with separate 50 Ω terminations attached to each input. Spectrums were recorded on the FFT with 800 points in the frequency range 10-100 kHz, well outside of the flicker noise regime out of the amplifiers.

The cross-spectrum of two signals, $a(t)$ and $b(t)$, is defined as the Fourier Transform of the cross-correlation function,

$$S^{ab}(f) = \mathcal{F}\left\{\lim_{\theta\to\infty}\frac{1}{\theta}\int_{\theta} a(t)b(t-\tau)dt\right\}. \tag{6}$$

However, experimentally we deal with digitzed signals such that $a(t)$ and $b(t)$ have been sampled and now contain N discrete values. The discrete cross-correlation function is

$$\mathrm{K}_{ab}^{(i)} = \frac{1}{N}\sum_{k=1}^{N} a_k b_{k+|i-N|}, \tag{7}$$

where the index i runs from 1 to $2N$. Hence the discrete implementation of eq. (6) is then

$$S^{ab}(f_i) = \mathcal{DF}\left\{\mathrm{K}_{ab}^{(i)}\right\}, \tag{8}$$

where $\mathcal{DF}$ is the discrete Fourier transform. The cross-power spectral density (X-PSD) can then be obtained by normalizing eq. (8) over the resolution bandwidth (i.e. multiplying by τ_{meas}).

We now consider the effect of averaging over m cross-spectrums. During this process if $a(t)$ and $b(t)$ contain any signals that are uncorrelated they will be rejected from the cross-spectrum at a rate proportional to $\sqrt{2m}$ [44, 45]. For most applications this rate of rejection is not observed as correlated signals have originated from a singular Device Under Test (DUT) which is then power-split and run through the two measurement channels, meaning that the ability to resolve the correlated signal of interest is only proportional to $\sqrt{m}$.

For a single channel measurement, the error (standard deviation) is reduced with $\sqrt{m}$ while the mean, μ, remains constant. In the cross-spectrum, the mean is reduced by $\sqrt{2m}$ while the error (standard deviation) remains proportionally constant relative to the mean. Once the limit of rejection is reached (generally set by the level of isolation between the two channels) then the standard deviation of the cross-spectrum starts to reduce. In the context of SNRs in WISP cavity receivers, lowering the uncertainty of the measurement and reducing the mean of the noise have the same effect. Most WISP searches are also unlikely to reach the limit of isolation between measurement channels.

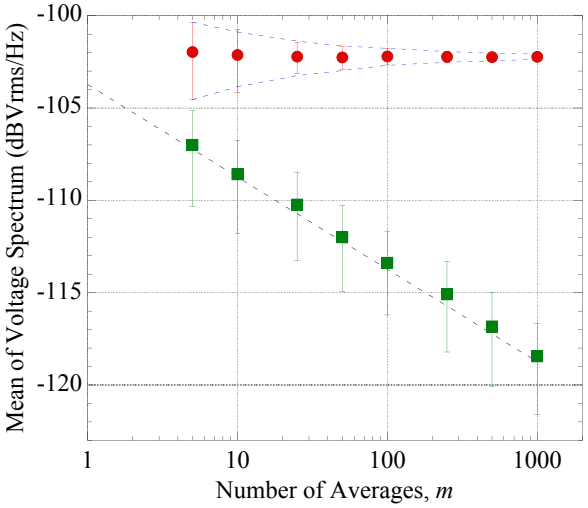

FIG. 3. Mean of voltage spectrums as a function of averages from the measurement scheme presented in Fig. 2. The mean of a single channel spectrum is shown (red circles) with error bars representing 1 standard deviation. A $\sqrt{m}$ dependence is shown (blue dashed line). The mean of the cross-spectrum is also shown (green squares) with error bars representing 1 standard deviation. The function $\mu_1/\sqrt{(2m)}$ is plotted (black dashed line) as discussed in the text.

We performed a simple measurement to demonstrate the principles of cross-correlation outlined in this section. Figure 2 shows the method used; data was collected for averages ranging from 5 to 1000. The mean of the single channel spectrum is shown (red circles) in Fig. 3 with the error bars representing 1 standard deviation. The $\sqrt{m}$ dependence of the error is shown by the dashed blue lines, while the mean (μ_1) stays constant. The mean value of the cross-spectrum (green circles) is also presented along with 1 standard deviation error bars. The function $\mu_1/\sqrt{2m}$ is plotted (black dashed line) and overlaps with the mean of the cross-spectrum, while the standard deviation of the cross-spectrum remains constant relative to the mean.

IV. CROSS-CORRELATION WISP CAVITY RECEIVER MEASUREMENT TECHNIQUES

Figure 4 outlines the first cross-correlation WISP cavity receiver technique. Two antennae probes are coupled to the microwave cavity, the output from each probe travels through nominally identical yet separate channels. After being mixed down to a lower frequency the spectrums are sampled on a FFT vector signal analyzer and the X-PSD is computed. In this scheme the broadband

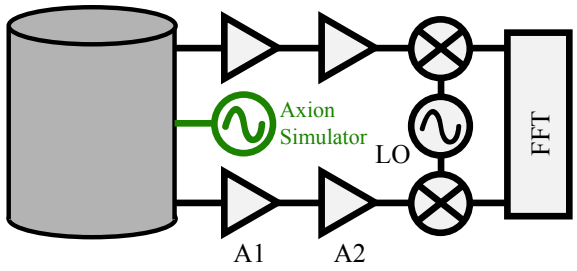

FIG. 4. Schematic of the first cross-correlation measurement technique. The axion simulator (green) is used in Sec. V to perform proof-of-concept measurements.

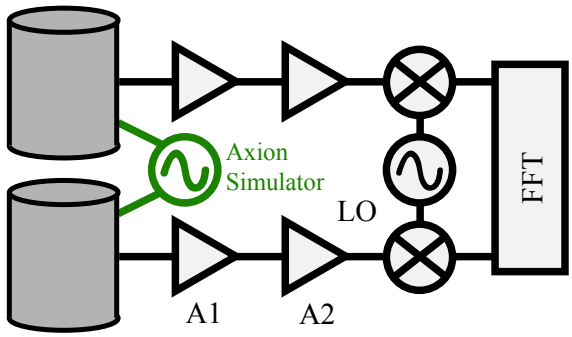

FIG. 5. Schematic of the second cross-correlation measurement technique. The axion simulator (green) is used in Sec. V to perform proof-of-concept measurements.

noise of the first-stage amplifiers, eq. (3), is rejected because it is thermal in origin and therefore uncorrelated. The power due to the thermal noise of the cavity and any WISP-to-photon conversion is correlated between both channels and thus retained in the cross-spectrum.

The ratio of power spectral densities can be represented as

$$\frac{\mathrm{S_P^{sig}}}{\mathrm{S_P^{cav}} + \frac{\sqrt{2}}{\sqrt{m}}\mathrm{S_P^{amp}}}. \tag{9}$$

Comparing eq. (9) to eq. (5), which scales with $\sqrt{m}$, it is clear that the single channel WISP cavity receiver has a higher SNR for a given number of averages. This cross-correlation method can be used to improve the contrast of the thermal cavity noise, which could allow for improved fits to the cavity noise spectrum, allowing one to better identify cavity parameters (such as Q-factor) which could well fluctuate over the course of an experiment, especially if the cavity is being frequency tuned. This technique may be of interest outside of WISP searches, for example in the characterization of high-Q cryogenic bulk acoustic wave resonators [46].

The second cross-correlation WISP cavity receiver technique is illustrated in Fig. 5. Here two separate nominally identical cavities each have a measurement channel coupled to them. This is different to other multiple-cavity WISP receivers, where the cavities are power-combined and then read out via a single measurement channel [47, 48]. When the cross-spectrum is computed on the FFT the first-stage amplifier noise and the thermal cavity noise is rejected, while a signal due to a flux of WISPs is correlated between the two cavities and thus remains in the cross-spectrum. This is only true when the cavities are not separated by a distance greater than the relevant de Broglie wavelength, which for axions is of the order 10-100 m [49]. As the noise being rejected is thermal (random), the performance of the system should be independent of the relative phase of the two measurement channels.

This technique does introduce the added complexity of having to tune the frequency of two independent cavities. Of course, the two cavities do not necessarily have to be tuned to overlap, the cross-spectrum will reject all cavity noise and retain an axion signal regardless of the relative frequencies (within reason), but to optimize the experiment the WISP mass should coincide with the resonant frequencies of the cavities. If one of the cavities was frequency detuned this can be treated as a reduction in the effective Q-factor of the cavity [27], which would reduce the amount of power generated in the cavity due to WISPs. As long as the cavities are not frequency detuned further apart than the bandwidth of the resonant cavity mode being used then this technique is still advantageous.

Assuming that the two cavities used are nominally idential to what would have been deployed in a single channel system, we can infer the ratio of PSDs for this readout system,

$$\sqrt{2m}\frac{\mathrm{S_P^{sig}}}{\mathrm{S_P^{cav}} + \mathrm{S_P^{amp}}}. \tag{10}$$

As the entire system noise ($\mathrm{S_P^{cav}} + \mathrm{S_P^{amp}}$) is rejected at the rate $\sqrt{2m}$, we see an improvement of $\sqrt{2}$ compared to a standard WISP cavity receiver, owing to the addition of the second cavity and measurement channel.

This cross-correlation technique would be useful in characterizing any candidate WISP signal. As each cavity output is immediately amplified it is possible to have the cavities separated by large spatial distances, while the standard power-summing approach requires the cavities to be co-located to avoid excessive losses along the individual transmission lines. Introducing amplifiers for each cavity would substantially increase the overall system noise. In contrast, the cavities in Fig. 5 can be spatially well separated and still maintain the same SNR. The cross-correlation measurement scheme could be used to scrutinize any candidate WISP signal and to measure the coherence length of a WISP, noting that as the cavities become separated by a distance greater than the coherence length of the particle, the generated power signal in each cavity will no longer be correlated and will be rejected from the cross-spectrum.

The scheme presented in Fig. 5 can be extrapolated to incorporate n cavities. In such a case, we can com-

pute the cross-spectrum of all the different possible combinations of cavities, resulting in $n\left(n-1\right)/2$ cross-spectrums. From this we can calculate the average X-PSD,

$$\mathrm{S_P^{ave}}\left(f_i\right) = \frac{2}{n\left(n-1\right)} \sum_{a=1}^{n-1} \sum_{b=a+1}^{n} \mathrm{S_P^{ab}}\left(f_i\right), \tag{11}$$

and infer the corresponding SNR as

$$\sqrt{mn\left(n-1\right)} \frac{\mathrm{S_P^{sig}}}{\mathrm{S_P^{cav}} + \mathrm{S_P^{amp}}}. \tag{12}$$

For comparison, considering the standard approach of coherently power-summing n cavities by connecting directly to a Wilkinson power combiner and then reading the output via a single amplification chain, we arrive at a SNR of

$$\sqrt{mn} \frac{\mathrm{S_P^{sig}}}{\mathrm{S_P^{cav}} + \frac{\mathrm{S_P^{amp}}}{\sqrt{n}}}. \tag{13}$$

Here we assume that the power combiner is noiseless, although it could be incorporated as an additional term in the denominator. If the cavity noise contribution is dominant relative to the amplifier noise ($\mathrm{S_P^{cav}} >> \mathrm{S_P^{amp}}$), then eq. (12) scales more favorably than eq. (13) for systems with 3 or more cavities. Alternatively, if the amplifier is the primary source of noise then eq. (13) offers a slight advantage over eq. (12).

It is worth highlighting that for axion searches the positioning of multiple cavities within the applied external magnetic field is non-trivial and can greatly impact upon the sensitivity of the WISP receiver [42].

V. RESULTS

Proof-of-concept measurements were made with both systems (Figs. 4 and 5). A microwave synthesizer was used to generate a simulated WISP signal that falls within the cavity bandwidth. Measurements were conducted at room temperature using sapphire dielectric-loaded copper cavities as they exhibit Q factors comparable to empty cryogenic copper cavities. As this is not an actual WISP search but rather a test of a measurement technique the mode structure of the cavity resonance is irrelevant. The cavities both had resonance frequencies at 9.3 GHz and Q factors of $\sim 5\times10^4$. The total gain in each channel was $\sim$60 dB and the power-to-voltage conversion efficiency of the mixers was $\sim$11 V/$\sqrt{\mathrm{W}}$. A microwave synthesizer was used to mix the channels down to 500 kHz so the spectrums could be recorded on the FFT.

Measurements were made from 50 to 1000 averages. With the appropriate equipment such as a FFT or multi-channel digitizer both channels can be sampled simultaneously and the cross-spectrum is computed in situ, meaning that there is no increase in acquisition time for cross-correlation measurements compared to single channel measurements.

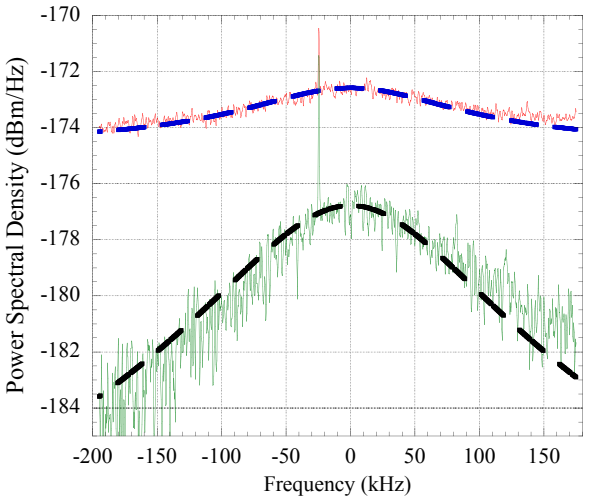

FIG. 6. A 1600 point PSD after 1000 averages for the first cross-correlation technique illustrated in Fig. 4. Single channel trace is shown in red, with expected result cavity and amplifier noise contribution given by the blue dashed line. The cross-spectrum is shown in green, with a fit to the data given by the dashed black line.

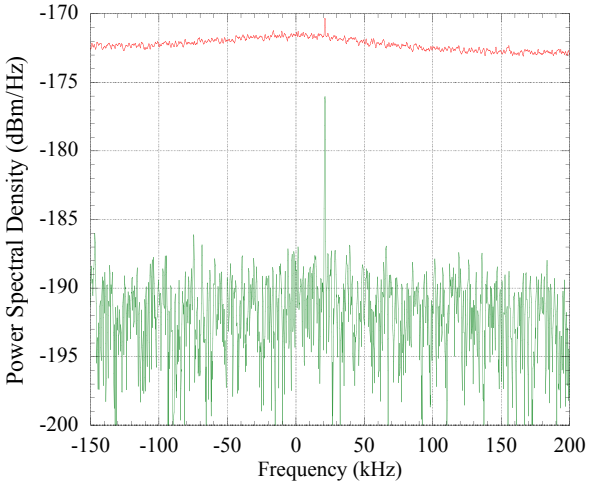

FIG. 7. A 1600 point PSD after 1000 averages for the second cross-correlation technique illustrated in Fig. 5. Single channel trace is shown in red and the X-PSD is shown in green.

The single channel PSD and dual channel X-PSD after 1000 averages for the first technique (Fig. 4) are shown in Fig. 6. The contrast of the thermal cavity noise has been enhanced in the X-PSD, owing to the rejection of the uncorrelated broadband amplifier noise. This demonstrates that the X-PSD conserves complex structures such as those expected for virialized CDM axions.

Here we will calculate the SNR as the ratio of the simulated signal PSD (i.e. maximum value) to the standard

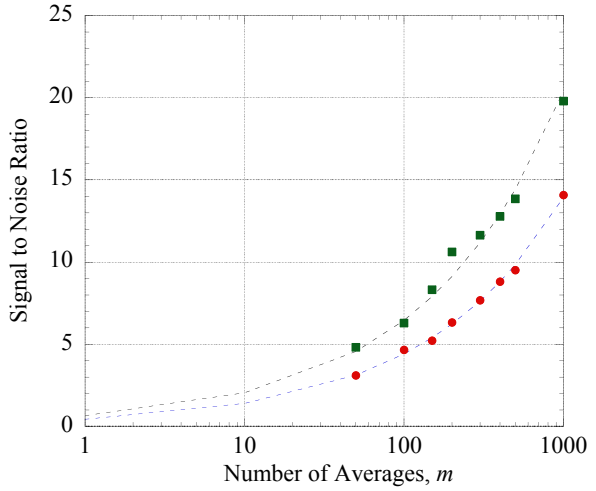

FIG. 8. Log-linear representation of SNR as a function of averages for the simulated axion signal in single channel (red circles) and X-PSD (green squares) obtained via the technique presented in Fig. 5. Fits to the data (dashed lines) are presented as discussed in the text.

deviation of the PSD. For frequency-dependent PSDs, such as the Lorentzian profiles of Fig. 7, fits and residuals are used to ensure a white PSD for analysis. For the single channel measurement, there is a linear SNR of 25σ, while for the dual channel measurement it is 32σ. Of course, the X-PSD SNR is only larger as the initial WISP and cavity power has been split between two channels; a true single-channel WISP receiver measurement would give a larger SNR.

Single channel and dual channel results for the second technique (Fig. 5) are shown in Fig. 7. Temperature control was used to perform minor frequency tuning to ensure that the resonant frequencies of both cavities were equal. After 1000 averages the single channel trace, representative of a typical WISP cavity receiver, has a linear SNR of 14σ for the WISP signal. In the X-PSD, the first-stage amplifier noise and thermal cavity noise from both channels has been rejected (within the limitations of the instrumentation and the number of averages taken). The simulated WISP signal which is correlated between both cavities remains with an enhanced SNR of 20σ, which is a factor of $\sqrt{2}$ improvement arising from the use of two independent measurement channels.

Figure 8 shows the SNR for a single channel and the X-PSD as a function of the number of averages taken. Fitting to the X-PSD gives the function $0.46\times\sqrt{2m}$ and fitting to a single channel gives $0.44\times\sqrt{m}$. This demonstrates that the system behaves as outlined in section IV and also shows that the X-PSD conserves relatively weak correlated signals, as the starting SNR for these measurements is less than 1.

For both measurement techniques the phase offset in each arm, or more importantly the phase difference between the two channels, ultimately has minimal impact upon the SNR observed in the X-PSD. As the noise processes being rejected are of thermal (random) origin the power will be equally distributed between phase and amplitude; we cannot further improve on the results by having a phase-sensitive channel and an amplitude-sensitive channel. Regardless, it would be prudent to fully characterize any system deployed in an actual data-taking experiment.

VI. CONCLUSION

Two cross-correlation measurement schemes for cavity-based WISP searches have been proposed and verified. The first scheme improves the resolution of the intrinsic thermal noise of the cavity. The second scheme allows for two cavity outputs to be effectively combined via computation of their cross-power spectral density. This scheme allows for the two cavities to be spatially well separated, thereby providing a way to measure the coherence length of any candidate WISP signal. Such an approach can be scaled up to larger arrays of cavities by computing all the possible combinations of cavity cross-power spectral densities.

ACKNOWLEDGMENTS

The authors thank J.M. Le-Floch for the data acquisition software. This work was supported by Australian Research Council grants DP130100205 and CE110001013.

[1] J. Jaeckel and A. Ringwald, Annual Review of Nuclear and Particle Science **60**, 405 (2010).
[2] R. D. Peccei and H. R. Quinn, Phys. Rev. Lett. **38**, 1440 (1977).
[3] S. Weinberg, Phys. Rev. Lett. **40**, 223 (1978).
[4] F. Wilczek, Phys. Rev. Lett. **40**, 279 (1978).
[5] J. E. Kim and G. Carosi, Rev. Mod. Phys. **82**, 557 (2010).
[6] L. Abbott and P. Sikivie, Physics Letters B **120**, 133 (1983).
[7] J. Preskill, M. B. Wise, and F. Wilczek, Physics Letters B **120**, 127 (1983).
[8] M. Dine and W. Fischler, Physics Letters B **120**, 137 (1983).
[9] J. Ipser and P. Sikivie, Phys. Rev. Lett. **50**, 925 (1983).
[10] S. Abel, M. Goodsell, J. Jaeckel, V. Khoze, and A. Ringwald, Journal of High Energy Physics **2008**, 124 (2008).
[11] M. Goodsell, J. Jaeckel, J. Redondo, and A. Ringwald, Journal of High Energy Physics **2009**, 027 (2009).
[12] B. Holdom, Physics Letters B **166**, 196 (1986).

[13] L. Okun, Sov.Phys.JETP **56**, 502 (1982).
[14] A. E. Nelson and J. Scholtz, Phys. Rev. D **84**, 103501 (2011).
[15] P. Arias, D. Cadamuro, M. Goodsell, J. Jaeckel, J. Redondo, and A. Ringwald, Journal of Cosmology and Astroparticle Physics **2012**, 013 (2012).
[16] P. Sikivie, Phys. Rev. Lett. **51**, 1415 (1983).
[17] P. Sikivie, Phys. Rev. D **32**, 2988 (1985).
[18] C. Hagmann, P. Sikivie, N. Sullivan, D. B. Tanner, and S.-I. Cho, Review of Scientific Instruments **61**, 1076 (1990).
[19] R. Bradley, J. Clarke, D. Kinion, L. J. Rosenberg, K. van Bibber, S. Matsuki, M. Mück, and P. Sikivie, Rev. Mod. Phys. **75**, 777 (2003).
[20] J. Jaeckel and A. Ringwald, Physics Letters B **659**, 509 (2008).
[21] P. W. Graham, J. Mardon, S. Rajendran, and Y. Zhao, Phys. Rev. D **90**, 075017 (2014).
[22] S. J. Asztalos, G. Carosi, C. Hagmann, D. Kinion, K. van Bibber, M. Hotz, L. J. Rosenberg, G. Rybka, J. Hoskins, J. Hwang, P. Sikivie, D. B. Tanner, R. Bradley, and J. Clarke, Phys. Rev. Lett. **104**, 041301 (2010).
[23] J. Hoskins, J. Hwang, C. Martin, P. Sikivie, N. S. Sullivan, D. B. Tanner, M. Hotz, L. J. Rosenberg, G. Rybka, A. Wagner, S. J. Asztalos, G. Carosi, C. Hagmann, D. Kinion, K. van Bibber, R. Bradley, and J. Clarke, Phys. Rev. D **84**, 121302 (2011).
[24] R. G. Povey, J. G. Hartnett, and M. E. Tobar, Phys. Rev. D **82**, 052003 (2010).
[25] A. Wagner, G. Rybka, M. Hotz, L. J. Rosenberg, S. J. Asztalos, G. Carosi, C. Hagmann, D. Kinion, K. van Bibber, J. Hoskins, C. Martin, P. Sikivie, D. B. Tanner, R. Bradley, and J. Clarke, Phys. Rev. Lett. **105**, 171801 (2010).
[26] M. Betz, F. Caspers, M. Gasior, M. Thumm, and S. W. Rieger, Phys. Rev. D **88**, 075014 (2013).
[27] S. R. Parker, J. G. Hartnett, R. G. Povey, and M. E. Tobar, Phys. Rev. D **88**, 112004 (2013).
[28] P. Slocum, O. Baker, J. Hirshfield, Y. Jiang, A. Malagon, A. Martin, S. Shchelkunov, and A. Szymkowiak, Nuclear Instruments and Methods in Physics Research Section A: Accelerators, Spectrometers, Detectors and Associated Equipment **770**, 76 (2015).
[29] C. Beck, Phys. Rev. Lett. **111**, 231801 (2013).
[30] R. G. Povey, J. G. Hartnett, and M. E. Tobar, Phys. Rev. D **84**, 055023 (2011).
[31] S. R. Parker, G. Rybka, and M. E. Tobar, Phys. Rev. D **87**, 115008 (2013).
[32] P. W. Graham and S. Rajendran, Phys. Rev. D **88**, 035023 (2013).
[33] R. Seviour, I. Bailey, N. Woollett, and P. Williams, Journal of Physics G: Nuclear and Particle Physics **41**, 035005 (2014).
[34] P. Sikivie, N. Sullivan, and D. B. Tanner, Phys. Rev. Lett. **112**, 131301 (2014).
[35] D. Budker, P. W. Graham, M. Ledbetter, S. Rajendran, and A. O. Sushkov, Phys. Rev. X **4**, 021030 (2014).
[36] A. Arvanitaki and A. A. Geraci, Phys. Rev. Lett. **113**, 161801 (2014).
[37] P. Sikivie, Phys. Rev. Lett. **113**, 201301 (2014).
[38] J. E. Kim, Phys. Rev. Lett. **43**, 103 (1979).
[39] M. Shifman, A. Vainshtein, and V. Zakharov, Nuclear Physics B **166**, 493 (1980).
[40] M. Dine, W. Fischler, and M. Srednicki, Physics Letters B **104**, 199 (1981).
[41] P. R. Kafle, S. Sharma, G. F. Lewis, and J. Bland-Hawthorn, The Astrophysical Journal **794**, 59 (2014).
[42] B. T. McAllister, S. R. Parker, and M. E. Tobar, "Axion dark matter coupling to resonant photons via magnetic field," (2015), arXiv:physics.hep-ph/1512.05547.
[43] W. Walls, in *Frequency Control Symposium, 1992. 46th., Proceedings of the 1992 IEEE* (1992) pp. 257 –261.
[44] E. Rubiola and V. Giordano, Rev. Sci. Instrum. **71**, 3085 (2000).
[45] E. Rubiola and F. Vernotte, "The cross-spectrum experimental method," arXiv:1003.0113v1.
[46] M. Goryachev, E. N. Ivanov, F. van Kann, S. Galliou, and M. E. Tobar, Applied Physics Letters **105**, 153505 (2014).
[47] S. Darin, *First results from a multiple-microwave-cavity search for dark-matter axions*, Ph.D. thesis, UC Davis (2001).
[48] T. M. Shokair, J. Root, K. A. Van Bibber, B. Brubaker, Y. V. Gurevich, S. B. Cahn, S. K. Lamoreaux, M. A. Anil, K. W. Lehnert, B. K. Mitchell, A. Reed, and G. Carosi, International Journal of Modern Physics A **29**, 1443004 (2014).
[49] G. Carois and K. V. Bibber, in *Lecture Notes in Physics - Axions: Theory, Cosmology, and Experimental Searches*, edited by M. Kuster, G. Raffelt, and B. Beltrán (Springer, 2008).